FADTTS: Functional Analysis of Diffusion Tensor Tract Statistics*

Hongtu Zhu[a,e], **Linglong Kong**[a], **Runze Li**[f], **Martin Styner**[b,c], **Guido Gerig**[g], **Weili Lin**[d,e], and **John H. Gilmore**[c]

[a] Department of Biostatistics, University of North Carolina at Chapel Hill, Chapel Hill, NC 27599, USA

[b] Department of Computer Science, University of North Carolina at Chapel Hill, Chapel Hill, NC 27599, USA

[c] Department of Psychiatry, University of North Carolina at Chapel Hill, Chapel Hill, NC 27599, USA

[d] Department of Radiology, University of North Carolina at Chapel Hill, Chapel Hill, NC 27599, USA

[e] Biomedical Research Imaging Center, University of North Carolina at Chapel Hill, Chapel Hill, NC 27599, USA

[f] Department of Statistics and The Methodology Center, The Pennsylvania State University, University Park, PA 16802, USA

[g] Scientific Computing and Imaging Institute, The University of Utah, Salt Lake City, Utah 84100, USA

Abstract

The aim of this paper is to present a functional analysis of diffusion tensor tract statistics (FADTTS) pipeline for delineating the association between multiple diffusion properties along major white matter fiber bundles with a set of covariates of interest, such as age, diagnostic status and gender, and the structure of the variability of these white matter tract properties in various diffusion tensor imaging studies. The FADTTS integrates five statistical tools: (i) a multivariate varying coefficient model for allowing the varying coefficient functions in terms of arc length to characterize the varying association between fiber bundle diffusion properties and a set of covariates, (ii) a weighted least squares estimation of the varying coefficient functions, (iii) a functional principal component analysis to delineate the structure of the variability in fiber bundle diffusion properties, (iv) a global test statistic to test hypotheses of interest, which may be associated with different diffusion properties, and (v) a simultaneous confidence band to quantify the uncertainty in the estimated coefficient functions. Simulated data are used to evaluate the finite sample performance of FADTTS. We also apply FADTTS to investigate the development of white

matter diffusivities along the splenium of the corpus callosum tract and the right internal capsule tract in a clinical study of neurodevelopment. FADTTS can be used to facilitate understanding of normal brain development, the neural bases of neuropsychiatric disorders, and the joint effects of environmental and genetic factors on white matter fiber bundles.

Keywords

Confidence band; diffusion tensor imaging; fiber bundle; global test statistic; varying coefficient model

1. Introduction

Diffusion tensor imaging (DTI), which can track the effective diffusion of water in the human brain in vivo, has been widely used to map the structure and orientation of the white matter fiber tracts of the brain (Basser et al., 1994a,b). In DTI, the degree of diffusivity and the directional dependence of water diffusion in each voxel can be quantified by a 3×3 matrix, called a diffusion tensor (DT), and its tensor-derived quantities, called diffusion properties, including the three eigenvalue-eigenvector pairs of DT and other related parameters, such as fractional anistropy (FA) (Pierpaoli and Basser, 1996; Hasan et al., 2001; Hasan and Narayana, 2003; Zhu et al., 2006). A wealth of neuroimaging studies have been conducted to use these tensor-derived quantities as a marker for white matter tract maturation and integrity in order to better understand normal brain development and the neural bases of neuropsychiatric and neuro-degenerative disorders (Moseley, 2002; Mukherjee and McKinstry, 2006; Cascio et al., 2007; Rollins, 2007).

In the current literature, there exist three major approaches to the group analysis of diffusion imaging data: region-of-interest (ROI) analysis, voxel based analysis, and fiber tract based analysis (Smith et al., 2006; O'Donnell et al., 2009; Snook et al., 2007). The ROI analysis used in some neuroimaging studies (Bonekam et al., 2008; Gilmore et al., 2008) primarily averages diffusion properties in some manually drawn ROIs for each subject and then creates a single statistic per ROI (Snook et al., 2007). The main drawbacks of ROI analysis are the difficulty in identifying meaningful ROIs, particularly the long curved structures common in fiber tracts, the instability of statistical results obtained from ROI analysis, and the partial volume effect in relative large ROIs (Goodlett et al., 2009; Zhu et al., 2010c). A stringent assumption of ROI analysis is that diffusion properties in all voxels of the same ROI are essentially homogeneous, which is largely false for DTI.

Voxel-based analysis is used more commonly than ROI analysis in neuroimaging studies (Chen et al., 2009; Focke et al., 2008; Camara et al., 2007; Snook et al., 2005). It usually involves fitting a statistical model to the smoothed and registered diffusion property imaging data from multiple subjects at each voxel to generate a parametric map of test statistics (or *p*-values). Subsequently, a multiple comparison procedure such as random field theory is applied to correct for multiple comparisons across the many voxels of the imaging volume (Ashburner and Friston, 2000; Wager et al., 2005; Worsley et al., 2004). The major drawbacks of voxel based analysis include poor alignment quality and the arbitrary choice of smoothing extent (Hecke et al., 2009; Ashburner and Friston, 2000; Smith et al., 2006; Jones et al., 2005). Particularly, extensive simulation results have shown that the final results of voxel based analysis can strongly depend on the amount of smoothing in the smoothed diffusion imaging data (Jones et al., 2005).

With the drawbacks of ROI and voxel based analyses, there is a growing interest in the DTI literature in developing fiber tract based analysis of diffusion properties (Smith et al., 2006;

O'Donnell et al., 2009; Yushkevich et al., 2008; Goodlett et al., 2009; Zhu et al., 2010c). For instance, a *tract based spatial statistics* framework was developed to construct local diffusion properties along the white matter skeleton and then perform pointwise hypothesis tests on the skeleton (Smith et al., 2006). A model based framework was developed for the statistical analysis of diffusion properties on the medial manifolds of fiber tracts followed by testing pointwise hypotheses on the medial manifolds (Yushkevich et al., 2008). These two methods essentially ignore the functional nature of diffusion properties in terms of arc length along the white skeleton and the medial manifolds, and thus they suffer from low statistical power in detecting interesting features and exploring variability in functional data. Statistically, diffusion properties along fiber bundles are functional data of position along the tract. Formal functional analysis of these fiber bundle diffusion properties requires recently developed advanced functional data analysis methods (Li and Hsing, 2010; Yao and Lee, 2006; Hall et al., 2006; Ramsay and Silverman, 2005, 2002).

There are several developments on the use of functional data analysis methods for the statistical analysis of diffusion properties along fiber tracts. A "smoothing first, then estimation" was proposed by Goodlett and his coauthors. They used the functional principal component analysis coupled with the Hotelling T^2 statistic to compare a univariate diffusion property, such as fractional anisotropy, across two (or more) populations for a single hypothesis test per tract (Goodlett et al., 2009; Ramsay and Silverman, 2005). The method is limited to a univariate diffusion property and cannot control for other continuous covariates of interest, such as age. The constraint principal component analysis method was used by Gouttard and his coauthors to fit the age related changes of diffusion properties along fiber tracts (Gouttard et al., 2009). Three major limitations of their method include that it only fits a univariate diffusion property; it cannot control for multiple covariates of interest, such as age and gender; and it cannot test a hypothesis of interest, such as age effect. Zhu and his coauthors presented a functional regression analysis of DTI tract statistics, called FRATS, for analyzing multiple diffusion properties along fiber bundles with a set of covariates of interest (Zhu et al., 2010c). FRATS is also "smoothing first, then estimation," and is executed in two steps (Zhu et al., 2010c; Zhang and Chen, 2007). The first step is to smooth multiple diffusion properties along individual fiber bundles by using the local polynomial kernel method. The second step is to fit a functional linear model with varying coefficient functions to directly characterize the association between the smoothed fiber bundle diffusion properties and a set of covariates, and then to test hypotheses of interest. However, their method is not capable of delineating the structure of the variability in fiber bundle diffusion properties or quantifying the uncertainty in the estimated coefficient functions. A multivariate varying coefficient model was developed by Zhu and his coauthors; it only includes coefficient estimating and hypotheses testing methods (Zhu et al., 2010b). Greven and her coauthors also developed a univariate varying coefficient model for longitudinal functional data, but they have not developed any formal statistics for testing hypotheses and constructing the confidence band of any varying coefficient function in a frequentist framework (Greven et al., 2010).

This paper is to develop a functional analysis of diffusion tensor tract statistics (FADTTS) pipeline for delineating the structure of the variability of multiple diffusion properties along major white matter fiber bundles and their association with a set of covariates. Diffusion properties, such as fractional anisotropy (FA) and mean diffusivity (MD), along fiber tracts are modeled as functions of the position along the tracts. Compared with the existing literature (Goodlett et al., 2009; Zhu et al., 2010c; Greven et al., 2010; Zhu et al., 2010b), there are five methodological contributions in this paper. First, a multivariate varying coefficient model is developed to characterize the association between fiber bundle diffusion properties and a set of covariates. Second, a weighted least squares estimation is proposed to directly estimate the varying coefficient functions without using the "smoothing first, then

estimation" strategy. Third, a functional principal component analysis is employed to delineate the structure of the variability in fiber bundle diffusion properties. Fourth, under the multivariate varying coefficient model, a global test statistic is proposed to test hypotheses of interest and a resampling method is developed for approximating the *p*-value of the global test statistic. Fifth, a simultaneous confidence band is built to quantify the uncertainty in the estimated coefficient functions and a resampling method is proposed to approximate the critical point. The advantages of FADTTS are that they are capable of modelling the structured inter-subject variability by a functional principal component analysis method, testing the joint effects by a global test statistic and local test statistics, and constructing simultaneous confidence bands of the interested effects through a resampling method. Moreover, compared to univariate analysis of the diffusion tensor tracts, the multivariate modeling is important for the testing of joint effects, but it is not crucial for estimation (Zellner, 1962).

2. Methodologies

The focus of this paper is to present a functional analysis pipeline, called FADTTS, with five powerful statistical tools for delineating the structure of the variability of multiple diffusion properties along major white matter fiber bundles and their association with a set of covariates of interest, such as age. Mathematically, we have rigorously derived the asymptotic properties of FADTTS, whose detailed assumptions and proofs are available from the first author upon request (Zhu et al., 2010a). A schematic overview of FADTTS is given in Fig. 1. The code for FADTTS was written in Matlab, which along with its documentation is freely accessible from our website http://www.bios.unc.edu/research/bias/software.html. To make it user-friendly, we developed a Graphical User Interface (GUI) to pack the code, also freely downloadable from the same website.

To compare diffusion properties in populations of DTIs, we use the DTI atlas building followed by atlas fiber tractography and fiber parametrization as described in Goodlett et al. (2009) to extract DTI fibers and establish DTI fiber correspondence across all DTI datasets from different subjects. Since this method has been described in detail (Goodlett et al., 2009; Zhu et al., 2010c), we skip its description here for the sake of simplicity. We briefly describe each component of FADTTS in the following subsections, and their technical details can be found in Zhu et al. (2010a).

2.1. Multivariate Varying Coefficient Model

We develop a *multivariate varying coefficient model* to model J diffusion quantities (e.g., FA) measured along fiber bundles with a set of covariates of interest. The J diffusion properties along fiber tracts are treated as functional data, which are functions of the position of the tracts and have no connection with functional magnetic resonance imaging data. Let $s \in [0, L]$ be the arc length of any point on a specific fiber bundle relative to a fixed end point of the fiber bundle, where L is the longest arc length on the fiber bundle. For the i-th subject, we consider an $J \times 1$ vector of diffusion properties, denoted by $\mathbf{y}_i(s_m) = (y_{i,1}(s_m), \cdots, y_{i,J}(s_m))^T$, and its associated arc length s_m for the m-th location grid point on the fiber bundle for $i = 1, \cdots, n$ and $m = 1, \cdots, M$, where n and M denote the numbers of subjects and grid points, respectively. We consider a multivariate varying coefficient model (Fan and Zhang, 1999; Wu and Chiang, 2000; Fan et al., 2003; Fan and Zhang, 2008; Wang et al., 2008; Ferguson et al., 2009), which assumes that for $i = 1, \cdots, n$ and $j = 1, \cdots, J$,

$$y_{ij}(s) = \mathbf{x}_i^T B_j(s) + \eta_{i,j}(s) + \varepsilon_{i,j}(s), \tag{1}$$

where $B_j(s) = (\beta_{j1}(s), \cdots, \beta_{jp}(s))^T$ is a $p \times 1$ vector of coefficient functions of arc length s, $\mathbf{x}_i$ is a $p \times 1$ vector of covariates of interest with $x_{i,1} = 1$, and $\varepsilon_{i,j}(s)$ are measurement errors.

Moreover, $\eta_{i,j}(s)$ characterizes both the individual curve variations from $\mathbf{x}_i^T B_j(s)$ and the correlation between $y_{i,j}(s)$ and $y_{i,j}(t)$ for different s and t. That is, $\eta_{i,j}(s)$ measures both subject-specific variability and location-specific variability. In addition, $\beta_{j1}(s)$ describes an average curve, i.e. a typical curve, of the j-th diffusion property.

It is also assumed that $\boldsymbol{\eta}_i(s) = (\eta_{i,1}(s), \cdots, \eta_{i,J}(s))^T$ and $\boldsymbol{\varepsilon}_i(s) = (\varepsilon_{i,1}(s), \cdots, \varepsilon_{i,J}(s))^T$ are mutually independent, and $\boldsymbol{\eta}_i(s)$ and $\boldsymbol{\varepsilon}_i(s)$ are, respectively, independent and identical copies of SP($\mathbf{0}, \Sigma_\eta$) and SP($\mathbf{0}, \Sigma_\varepsilon$), where SP($\mu, \Sigma$) denotes a vector with elements being stochastic processes with mean function $\mu(s)$ and covariance function $\Sigma(s, t)$ for any $s, t \in [0, L]$. Moreover, for any $1 \le u, v \le M$, the covariance structure of $\mathbf{y}_i(s)$, denoted by $\Sigma_y(s, t) = (\Sigma_{y,uv}(s, t))$, is given by

$$\sum\nolimits_{y,uv}(s,t) = \mathrm{Cov}(\mathbf{y}_{i,u}(s), \mathbf{y}_{i,v}(t)) = \sum\nolimits_{\eta,uv}(s,t) + \sum\nolimits_{\varepsilon,uv}(s,t)\mathbf{1}(s=t),$$

(2)

where $\Sigma_{\eta,uv}(s, t)$ and $\Sigma_{\varepsilon,uv}(s, t)$ are the (u, v)-th component of $M \times M$ matrices $\Sigma_\eta(s, t)$ and $\Sigma_\varepsilon(s, t)$, respectively.

Since the design matrix is the same for all diffusion properties, the estimators of $B_j(s)$ for $j = 1, 2, \cdots, J$ from (1) by pooling all diffusion properties together are identical to those obtained by fitting diffusion properties individually (Zellner, 1962). However, the covariance structure of $\mathbf{y}_i(s)$ plays an essential role in the inference procedure (e.g. hypotheeis testing and constructing confidence bands), which can only be estimated by pooling all diffusion properties together using model (1). Moreover, in practice, it is also interested to compare different tensor-derived statistics along the tract, and thus a functional analysis method for multiple outcomes is necessary and useful. For instance, in real data analysis, one may be interested in testing which eigenvalue grows faster (Zhu et al., 2010c).

As an illustration, in our clinical study on early brain development, we are interested in studying the evolution of the three eigenvalues L$_j$, $j = 1, 2, 3$, of diffusion tensor (L$_1 \ge$ L$_2 \ge$ L$_3$) along two selected fiber tracts in 128 healthy pediatric subjects (Figs. 4(a) and 8(a)). We consider a multivariate varying coefficient model of the three eigenvalues along a specific tract as follows:

$$\begin{aligned}
\mathrm{L}_{i,1}(s) &= \beta_{11}(s) + \beta_{12}(s) \times \mathrm{G}_i + \beta_{13}(s) \times \mathrm{Gage}_i + \eta_{i,1}(s) + \varepsilon_{i,1}(s), \\
\mathrm{L}_{i,2}(s) &= \beta_{21}(s) + \beta_{22}(s) \times \mathrm{G}_i + \beta_{23}(s) \times \mathrm{Gage}_i + \eta_{i,2}(s) + \varepsilon_{i,2}(s), \\
\mathrm{L}_{i,3}(s) &= \beta_{31}(s) + \beta_{32}(s) \times \mathrm{G}_i + \beta_{33}(s) \times \mathrm{Gage}_i + \eta_{i,3}(s) + \varepsilon_{i,3}(s),
\end{aligned}$$

(3)

where L$_{i,j}(s)$ equals L$_j$ at the location s for $j = 1, 2, 3$ and $i = 1, \cdots, 128$ and G$_i$ and Gage$_i$, respectively, denote the gender and the gestational age at the scan time of the i-th infant. In this case, $J = 3$, $B_j(s) = (\beta_{j1}(s), \beta_{j2}(s), \beta_{j3}(s))^T$, and $\mathbf{x}_i = (1, \mathrm{G}_i, \mathrm{Gage}_i)^T$.

2.2. Weighted Least Squares Estimation

To estimate the coefficient functions in $\mathbf{B}(s) = [B_1(s), B_2(s), \cdots, B_J(s)]$, we employ a weighted least squares (WLS) method based on a local polynomial kernel (LPK) smoothing technique (Fan and Gijbels, 1996; Wand and Jones, 1995; Wu and Zhang, 2006; Ramsay and Silverman, 2005; Welsh and Yee, 2006; Zhang and Chen, 2007). Specifically, using Taylor's expansion, we can expand $B_j(s_m)$ at s to obtain

$$B_j(s_m) \approx B_j(s) + \dot{B}_j(s)(s_m - s), \tag{4}$$

where $\dot{B}_j(s) = (\beta_{j1}(s), \cdots, \beta_{jp}(s))^T$ and $\beta_{jl}(s) = d\beta_{jl}(s)/ds$ for $l = 1, \cdots, p$. Let $K(\cdot)$ be a kernel function, such as the Gaussian and uniform kernels (Fan and Gijbels, 1996; Wand and Jones, 1995). For each j and a fixed bandwidth h, the weighted least square estimator of $B_j(s)$ is obtained by minimizing an objective function

$$\sum_{i=1}^{n} \sum_{m=1}^{M} [y_{i,j}(s_m) - \mathbf{x}_i^T A_j(h, s_m - s)\mathbf{z}(h, s_m - s)]^2 K((s_m - s)/h)/h, \tag{5}$$

where $A_j(h, s_m - s) = [B_j(s), h\dot{B}_j(s)(s_m - s)]$ and $\mathbf{z}(h, s_m - s) = (1, (s_m - s)/h)^T$. The WLS method differs from the standard least squares method by only incorporating observations measured at those grid points near each point s.

To select an optimal bandwidth, we use a leave-one-out generalized cross-validation score method for simplicity and computational efficiency (Zhang and Chen, 2007; Zhu et al., 2010a). Other bandwidth selection methods, such as Bayesian evidence optimization, can be implemented directly as well. In practice, we standardize all covariates and diffusion properties to have mean zero and standard deviation one and then choose a common bandwidth for all covariates, which greatly increases computational efficiency in bandwidth selection. Moreover, the estimation results are fairly robust to the bandwidth selection unless an extremely small or large bandwidth is chosen. Based on our experience in simulation studies, we recommend searching around $\max\{30, M/2\}$ log-spaced points from $1/M$ to $1/8$ of the arc length range. For each diffusion property, we select an optimal bandwidth and compute the corresponding estimator of $B_j(s)$, denoted by $\hat{B}_j(s)$, at the optimal bandwidth.

2.3. Functional Principal Component Analysis

To simultaneously construct all individual variation functions $\eta_{i,j}(s)$, we also employ the local polynomial kernel smoothing technique (Fan and Gijbels, 1996; Wand and Jones, 1995; Wu and Zhang, 2006; Ramsay and Silverman, 2005; Welsh and Yee, 2006; Zhang and Chen, 2007). Specifically, using Taylor's expansion, we can expand $\eta_{i,j}(s_m)$ at s to obtain $\eta_{i,j}(s_m) \approx \eta_{i,j}(s) + \dot{\eta}_{i,j}(s)(s_m - s)$. We develop an algorithm based on WLS with LPK to estimate $\eta_{i,j}(s)$ as follows. For each j and a fixed bandwidth h, we estimate $\eta_{i,j}(s)$ by minimizing an objective function

$$\sum_{m=1}^{M} [y_{i,j}(s_m) - \mathbf{x}_i^T \widehat{B}_j(s_m) - D_{i,j}(h, s_m - s)\mathbf{z}(h, s_m - s)]^2 K((s_m - s)/h)/h, \tag{6}$$

where $D_{i,j}(h, s_m - s) = [\eta_{i,j}(s), h\dot{\eta}_{i,j}(s)(s_m - s)]$.

Pooling all the data from n subjects for each j, the optimal bandwidth is selected by using a leave-one-out generalized cross-validation score method. Based on the optimal bandwidth, we estimate $\eta_{i,j}(s)$ and $\boldsymbol{\eta}_i(s)$, denoted by $\hat{\eta}_{i,j}(s)$ and $\hat{\boldsymbol{\eta}}_i(s)$, respectively, for all i and j. We then use their empirical mean and covariance to estimate $\boldsymbol{\eta}(s)$ and $\Sigma_\eta(s, t)$. The estimator of $\Sigma_\varepsilon(s, s)$ is a weighted mean of the empirical covariances of $\hat{\varepsilon}_i(s_m) = \mathbf{y}_i(s_m) - \hat{B}(s_m)^T \mathbf{x}_i - \hat{\boldsymbol{\eta}}_i(s_m)$ by a kernel approach with the optimal bandwidth selected by a cross validation method.

Functional principal component analysis (FPCA) attempts to find the dominant modes of variation around regression functions, and is thus a key technique in functional data analysis (Li and Hsing, 2010; Yao and Lee, 2006; Hall et al., 2006; Ramsay and Silverman, 2005, 2002). We calculate the spectral decomposition of $\hat{\Sigma}_{\eta,jj}(s, t)$ for each j as follows:

$$\widehat{\sum}_{\eta,jj}(s, t) = \sum_{l=1}^{\infty} \widehat{\lambda}_{j,l} \widehat{\psi}_{j,l}(s) \widehat{\psi}_{j,l}(t),$$

(7)

where $\hat{\lambda}_{j,1} \geq \hat{\lambda}_{j,2} \geq \cdots \geq 0$ are estimated eigenvalues and the $\hat{\psi}_{j,l}(t)$'s are the corresponding estimated principal components. For finite M, we essentially have a regular principal component analysis (PCA). That is, we have a finite number of estimated non-zero eigenvalues, which are the eigenvalues of $(\hat{\Sigma}_{\eta,jj}(s_u, s_v))$ for $u, v = 1, \cdots, M$, and the estimated principal components $[\hat{\psi}_{j,l}(s_1), \cdots, \hat{\psi}_{j,l}(s_M)]$ are the l-th eigenfunction of $(\hat{\Sigma}_{\eta,jj}(s_u, s_v))$. In practice, we use the rule that the proportion of variance explained is greater than 80% to truncate eigenvalues.

2.4. Hypothesis Test

In neuroimaging studies, most scientific questions require the comparison of fiber bundle diffusion properties along fiber bundles across two (or more) diagnostic groups and the assessment of the development of fiber bundle diffusion properties across age. Such questions can often be formulated as linear hypotheses of $B(s)$ as follows:

$$H_0 : \mathbf{C}\text{vec}(B(s)) = \mathbf{b}_0(s) \text{ for all } s \text{ vs. } H_1 : \mathbf{C}\text{vec}(B(s)) \neq \mathbf{b}_0(s),$$

(8)

where $\mathbf{C}$ is a $r \times Jp$ matrix of full row rank and $\mathbf{b}_0(s)$ is a given $r \times 1$ vector of functions.

As an illustration, in model (3), we are interested in comparing the evolution speeds of the three eigenvalues of the diffusion tenors along selected fiber tracts in 128 healthy pediatric subjects in our clinical study on early brain development. Statistically, for model (3), the comparison can be formulated as follows:

$$H_0 : \beta_{13}(s) = \beta_{23}(s) = \beta_{33}(s) \text{ for all } s \text{ vs.}$$
$$H_1 : |\beta_{13}(s) - \beta_{23}(s)| + |\beta_{23}(s) - \beta_{33}(s)| \neq 0.$$

In this case, we have

$$\mathbf{C} = \begin{pmatrix} 0 & 0 & 1 & 0 & 0 & 0 & 0 & 0 & -1 \\ 0 & 0 & 0 & 0 & 0 & 1 & 0 & 0 & -1 \end{pmatrix} \text{ and } \mathbf{b}_0(s) \equiv \begin{pmatrix} 0 \\ 0 \end{pmatrix} \text{ for all } s.$$

The use of multiple diffusion properties in model (3) allows us to compare different functions in B(s) associated with different diffusion properties.

We propose both local and global test statistics. The local test statistic can identify the exact location of a significant grid point on a specific tract. At a given grid point s_m on a specific tract, we test the local null hypothesis $H_0(s_m)$: $\mathbf{C}\text{vec}(B(s_m)) = \mathbf{b}_0(s_m)$ against $H_1(s_m)$: $\mathbf{C}\text{vec}(B(s_m)) \neq \mathbf{b}_0(s_m)$. The local test statistic $S_n(s_m)$ is defined by

$$S_n(s_m) = \mathbf{d}(s_m)^T [\mathbf{C}(\widehat{\sum}_\eta(s_m, s_m) \otimes \widehat{\Omega}_x^{-1})\mathbf{C}^T]^{-1} \mathbf{d}(s_m),$$

(9)

where $\widehat{\Omega}_x^{-1} \sum_{i=1}^n \mathbf{x}_i^{\otimes 2}$, $\mathbf{d}(s) = \mathbf{C}\text{vec}(\hat{B}(s) - \text{bias}(\hat{B}(s))) - \mathbf{b}_0(s)$ and $\otimes$ denote the Kronecker product. Following Fan and Zhang (2000), a smaller bandwidth leads to a small value of bias($\hat{B}(s)$); thus, we drop bias($\hat{B}(s)$) from now on. We test the global null hypothesis H_0: $\mathbf{C}\text{vec}(B(s)) = \mathbf{b}_0(s)$ for all s using a global test statistic S_n defined by

$$S_n = \int_0^{L_0} \mathbf{d}(s)^T [\mathbf{C}(\widehat{\sum}_\eta(s, s) \otimes \widehat{\Omega}_x^{-1})\mathbf{C}^T]^{-1} \mathbf{d}(s)ds.$$

(10)

In order to use S_n as a test statistic, we have already shown that S_n has a desirable asymptotic distribution, a weighted χ^2 distribution. To efficiently approximate the *p*-value of S_n, we use a wild bootstrap method from Zhu et al. (2010a).

2.5. Confidence Bands

For a given significance level α, we construct a simultaneous confidence band for each coefficient function $\beta_{jl}(s)$ such that

$$P(\widehat{\beta}_{jl}^{L,\alpha}(s) < \beta_{jl}(s) < \widehat{\beta}_{jl}^{U,\alpha}(s) \text{ for all } s \in [0, L]) = 1 - \alpha,$$

(11)

where $\widehat{\beta}_{jl}^{L,\alpha}(s)$ and $\widehat{\beta}_{jl}^{U,\alpha}(s)$ are the lower and upper limits of the confidence band. Since $\sup_{s\in[0,L]} |\sqrt{n}[\widehat{\beta}_{jl}(s) - \beta_{jl}(s)]|$ converges in distribution to $\sup_{s\in[0,L]} |G_{jl}(s)|$, where $G_{jl}(\cdot)$ is a centered Gaussian process, we define the critical point $C_{jl}(\alpha)$ such that $P(\sup_{s\in[0,L]} |G_{jl}(s)| \le C_{jl}(\alpha)) = 1 - \alpha$. Therefore, a $1 - \alpha$ simultaneous confidence band for $\beta_{jl}(s)$ is given as follows:

$$\left(\widehat{\beta}_{jl}(s) - \frac{C_{jl}(\alpha)}{\sqrt{n}}, \quad \widehat{\beta}_{jl}(s) + \frac{C_{jl}(\alpha)}{\sqrt{n}}\right).$$

(12)

We develop an efficient resampling method to approximate $C_{jl}(\alpha)$ as in Zhu et al. (2007a) and Kosorok (2003).

3. Simulation Studies and A Real Example

We use two sets of Monte Carlo simulations and a real example to evaluate the finite-sample performance of FADTTS. All computations for these numerical examples were done in matlab on an IBM ThinkCentre M50 workstation. The computation for FADTTS is relatively efficient for moderate and even large data. For example, for our real example with $n = 128$, $J = 5$, $M = 75$ and $p = 3$, the whole FADTTS procedure including 500 wild bootstrap samples took an average CPU time of about 13 minutes. The computational time for FADTTS can be further reduced by using other computer languages, such as C++.

3.1. Simulation Studies

We conducted two sets of Monte Carlo simulations to evaluate the Types I and II error rates of the global test statistic S_n and the coverage probabilities of the simultaneous confidence bands of the functional coefficients B(s), respectively. In the first set of simulations, we evaluated the Types I and II error rates by simulating FA and MD measures (Fig. 8(b) and (c)) along the right internal capsule tract according to

$$(FA_i(s_m), MD_i(s_m))^T = (\mathbf{x}_i^T B_1(s_m), \mathbf{x}_i^T B_2(s_m))^T + \eta_i(s_m) + \varepsilon_i(s_m),$$
$$\mathbf{x}_i^T B_1(s) = \beta_{11}(s) + \beta_{12}(s) \times G_i + \beta_{13}(s) \times Gage_i,$$
$$\mathbf{x}_i^T B_2(s) = \beta_{21}(s) + \beta_{22}(s) \times G_i + \beta_{23}(s) \times Gage_i,$$

(13)

where G_i and $Gage_i$, respectively, denote gender and the gestational age at the scan time of the i-th infant; $\boldsymbol{\eta}_i(s) = (\eta_{i1}(s), \eta_{i2}(s))^T$ is a Gaussian process with zero mean and covariance matrix $\Sigma_\eta(s, t)$; and $\boldsymbol{\varepsilon}_i(s) = (\varepsilon_{i1}(s), \varepsilon_{i2}(s))^T$ is a Gaussian random vector with zero mean and covariance matrix $\Sigma_\varepsilon(s, t)\mathbf{1}(s = t)$. We used the FA and MD measures along the right internal capsule tract from all the 128 infants in our clinical data to estimate $\hat{B}(s)$ of B(s), $\hat{\boldsymbol{\eta}}(s)$ of $\boldsymbol{\eta}(s)$, and $\hat{\boldsymbol{\varepsilon}}(s)$ of $\boldsymbol{\varepsilon}(s)$ via $\hat{\boldsymbol{\varepsilon}}(s) = (FA(s), MD(s))^T - \hat{B}(s)^T\mathbf{x} - \hat{\boldsymbol{\eta}}(s)$. We fixed all the parameters at their values obtained from our clinical data, except that we assumed $(\beta_{13}(s), \beta_{23}(s)) = c(\hat{\beta}_{13}(s), \hat{\beta}_{23}(s))$, where c is a scalar specified below and $(\hat{\beta}_{13}(s), \hat{\beta}_{23}(s))$ were estimators obtained from our clinical data. To mimic imaging data, we generated random samples $\tau_i^{(g)}$ and $\tau_i(s_m)^{(g)}$ from a $N(0, 1)$ generator for $i = 1, \cdots, n$ and $m = 1, \cdots, M$ and then constructed

$$FA_i(s_m)^{(g)} = \hat{\beta}_{11}(s_m) + \hat{\beta}_{12}(s_m) \times G_i + c\hat{\beta}_{13}(s_m) \times Gage_i + \tau_i^{(g)}\hat{\eta}_{i1}(s_m) + \tau_i(s_m)^{(g)}\hat{\varepsilon}_{i1}(s_m),$$
$$MD_i(s_m)^{(g)} = \hat{\beta}_{21}(s_m) + \hat{\beta}_{22}(s_m) \times G_i + c\hat{\beta}_{23}(s_m) \times Gage_i + \tau_i^{(g)}\hat{\eta}_{i2}(s_m) + \tau_i(s_m)^{(g)}\hat{\varepsilon}_{i2}(s_m).$$

Our tests were based on the simulated values of FA and MD measures $FA_i(s_m)^{(g)}$ and $MD_i(s_m)^{(g)}$ for $i = 1, \cdots, n$ and $m = 1, \cdots, M$.

As already mentioned, in neuroimaging studies, a lot of scientific questions require assessment of the development of fiber bundle diffusion properties across age. In this simulation study, we formulated the questions as hypotheses test $H_0: \beta_{13}(s) = \beta_{23}(s) = 0$ for all s along the right internal capsule tract against $H_1: \beta_{13}(s) \neq 0$ or $\beta_{23}(s) \neq 0$ for at least one s on the tract. We first assumed $c = 0$ to assess the Type I error rates for the global test statistic S_n, and then we assumed $c = 0.2, 0.4, 0.6,$ and 0.8 to examine the Type II error rates for S_n at different effect sizes. In both cases,

$$\mathbf{C} = \begin{pmatrix} 0 & 0 & 1 & 0 & 0 & 0 \\ 0 & 0 & 0 & 0 & 0 & 1 \end{pmatrix} \text{ and } \mathbf{b}_0(s) \equiv \begin{pmatrix} 0 \\ 0 \end{pmatrix} \text{ for all } s.$$

To evaluate the Types I and II error rates at different sample sizes, we let $n = 128$ and 64. For $n = 128$, the values of gender and gestational age were set the same as the 128 infants in our clinical study. For $n = 64$, we randomly chose 32 males and 32 females from the 128 infants and used their values for gender and gestational age to simulate the values of FA and MD along the right internal capsule tract. Note that the number of grid points on the right internal capsule is 75 for both cases.

We applied FADTTS to the simulated values of FA and MD. Particularly, we approximated the p-value of S_n using the wild bootstrap method. For each simulation, the significance levels were set at $\alpha = 0.05$ and 0.01, and 500 replications were used to estimate the rejection rates. For a fixed α, if the Type I rejection rate is smaller than α, then the test is conservative, whereas if the Type I rejection rate is greater than α, then the test is anticonservative, or liberal. The Monte Carlo error rate is $\sqrt{\alpha(1-\alpha)/N}$ with $N = 500$.

As shown in Table 1, the rejection rates for S_n based on the resampling method are relatively accurate for all sample sizes ($n = 64$, or 128) and all effect sizes ($c = 0, 0.2, 0.4, 0.6$, or 0.8) at both significance levels ($\alpha = 0.01$ or 0.05) (Fig. 2(a) and (b): $n = 64$ and Fig. 2(c) and (d): $n = 128$). The statistical power for rejecting the null hypothesis increases with the sample size and the effect size, which is consistent with our expectation. In addition to that, to show that FADTTS outperforms GLM, we also analyzed the simulated data using general linear model (GLM), in which we fitted GLM at each s_m without $\eta_{i,j}(s_m)$. That is, standard GLM ignores the correlation among the data at different grid points. Then, we calculated the global testing statistic except that we replaced $\hat{\Sigma}_\eta(s_m, s_m)$ in S_n with $\hat{\Sigma}_y(s_m, s_m)$. Finally, we calculated the p-values by the wild bootstrap method as in FADTTS. Table 1 shows that GLM is much less powerful than FADTTS; see also Fig. 2. An advantage of using FADTTS is that it is capable of explicitly modelling the structured inter-subject variability, in addition to a standard white noise model. Therefore, although the parameter estimators calculated from the two methods are close to each other, the covariance estimate of these parameter estimators in GLM are larger than those in FADTTS.

We carried out the second set of Monte Carlo simulations to evaluate the coverage probabilities of the confidence bands for regression coefficients. For simplicity, we only simulated the MD measure along the right internal capsule tract (Fig. 8(c)) according to

$$\mathrm{MD}_i(s_m) = \beta_1(s_m) + \beta_2(s_m) \times \mathrm{G}_i + \beta_3(s_m) \times \mathrm{Gage}_i + \eta_i(s_m) + \varepsilon_i(s_m), \tag{14}$$

where $\eta_i(s)$ is a Gaussian process with zero mean and covariance $\sigma_\eta(s, t)$ and $\varepsilon_i(s)$ is a Gaussian random variable with zero mean and covariance $\sigma_\varepsilon(s, t)1(s = t)$. We used the MD measure along the right internal capsule tract from all 128 infants in our clinical study to estimate $\hat{B}(s)$ of $B(s)$, $\hat{\eta}(s)$ of $\eta(s)$, and $\hat{\varepsilon}(s)$ of $\varepsilon(s)$, respectively. We fixed all the parameters at their estimated values and assumed them to be the true values. Subsequently, we generated random samples τ_i and $\tau_i(s_m)$ from a $N(0, 1)$ generator for $i = 1, \cdots, n$ and $m = 1, \cdots, M$ and then constructed

$$\mathrm{MD}_i(s_m)^{(g)} = \widehat{\beta_1}(s_m) + \widehat{\beta_2}(s_m) \times \mathrm{G}_i + \widehat{\beta_3}(s_m) \times \mathrm{Gage}_i + \tau_i \widehat{\eta_i}(s_m) + \tau_i(s_m)\widehat{\varepsilon_i}(s_m).$$

Then, based on the generated MD values $\mathrm{MD}_i(s_m)^{(g)}$ for $i = 1, \cdots, n$ and $m = 1, \cdots, M$, we calculated the simultaneous confidence bands of functional coefficients $\hat{\beta}_1(s)$, $\hat{\beta}_2(s)$ and $\hat{\beta}_3(s)$ for all s. The 95% and 99% simultaneous confidence bands were considered. As noted by Fan and Zhang (2000), Ghouch and Genton (2009), and among many others, an appropriate smaller bandwidth would improve the coverage probabilities of the confidence bands. In our simulations, we found that a shrinkage factor of 0.8 generally works well. For simplicity and computational efficiency, we do not consider estimating the bias of $\hat{\beta}(s)$.

Based on 1, 000 simulated data sets, the empirical coverage probabilities of $\hat{\beta}_1(s)$, $\hat{\beta}_2(s)$ and $\hat{\beta}_3(s)$ for the significance level $\alpha = 0.01$ (or $\alpha = 0.05$) are, respectively, 0.991, 0.994, and

0.978 (0.948, 0.952 and 0.926). The coverage probabilities are quite close to the claimed confidence levels. Figs. 5 and 9 depict typical simultaneous confidence bands.

3.2. A Real Example

This clinical study was approved by the Institutional Review Board of the University of North Carolina at Chapel Hill. A total of 128 healthy full-term infants (75 males and 53 females) were taken from a larger study designated to investigate early brain development at our institution. All 128 infants were less than one year old, and the written informed consent was obtained from their parents before imaging acquisition. The mean gestational age at MR scanning of the 128 infants was 298 ± 17.6 days (range: 262 to 433 days). All infants were fed and calmed to sleep on a warm blanket with proper ear protection. Technicians ensured that they slept comfortably inside the MR scanner, and thus none of them was sedated during the imaging session.

A 3T Allegra head-only MR system (Siemens Medical Inc., Erlangen, Germany) was used to acquire all the images. The system was equipped with a maximal gradient strength of 40 mT/m and a maximal slew rate of 400 mT/(m·msec). The DTI images were obtained by using a single shot EPI DTI sequence (TR/TE=5400/73 msec) with eddy current compensation. We applied the six non-collinear directions at the b-value of 1000 s/mm^2 with a reference scan ($b = 0$). The voxel resolution was isotropic 2 mm, and the in-plane field of view was set at 256 mm in both directions. To improve the signal-to-noise ratio of the images, a total of five scans were acquired and averaged.

To construct the diffusion tensors, we used a weighted least squares estimation method (Zhu et al., 2007b; Basser et al., 1994a). We then employed our DTI atlas building followed by an atlas-based tractography procedure to process all 128 DTI datasets. While several DTI fiber tracts were tracked, we chose to focus in this paper on the splenium of the corpus callosum and the right internal capsule tract to illustrate the applicability of our method (Figs. 4 and 8). Five diffusion properties were extracted along the selected fiber tracts including ractional anistropy (FA), mean diffusivity (MD), and the three eigenvalues of the diffusion tensors, denoted by $L_1 \geq L_2 \geq L_3$, at each grid point along all fiber tracts of interest for all the 128 infants (Goodlett et al., 2009). FA and MD, respectively, measure the inhomogeneous extent of local barriers to water diffusion and the averaged magnitude of local water diffusion, while L_js ($j = 1, 2, 3$) reflect the magnitude of water diffusivity along and perpendicular to the long axis of white matter fibers (Song et al., 2003).

In this study, we have two specific aims. The first one is to compare diffusion properties along the selected fiber bundles across the male and female groups and thus illuminate the gender effect on the development of these fiber bundle diffusion properties. The second one is to delineate the development of fiber bundle diffusion properties across time—the age effect. As a graphical illustration, we plotted FA measures along the right internal capsule tract from 40 randomly selected infants (Fig. 3). We observed that the values of FA increase with gestational age at nearly all grid points. To statistically test the gender and age effects, we applied FADTTS to the joint analysis of FA and MD values and the three eigenvalues along each of the two tracts.

For the two selected tracts, we fit the multivariate varying coefficient model (1) to the smoothed FA and MD values and the three eigenvalues from all 128 subjects, in which $\mathbf{x} = (1, G, Gage)^T$ and $M = 5$. We then estimated the functional coefficients B(s). In the functional principal component analysis part, we estimated $\boldsymbol{\eta}(s)$ and constructed the spectral decomposition of $\hat{\Sigma}_{\eta,jj}(s, t)$ for all $j = 1, \cdots, J$ by calculating their eigenvalues and eigenfunctions. For the hypothesis testing, we constructed the global test statistic S_n via equation (10) to test the gender and age effects for the five diffusion-tensor properties

altogether. We approximated the *p*-value of S_n using the resampling method with $G = 1,000$ replications. Finally, we constructed the 95% simultaneous confidence bands for the functional coefficients B(*s*).

The bandwidths selected by GCV for the five diffusion properties along the right internal capsule tract are, respectively, 0.49, 0.68, 0.63, 0.74 and 0.58. Fig. 5 presents the estimated varying functional coefficients $\hat{B}(s)$ associated with all five diffusion properties (blue solid lines in all panels of Fig. 5). The intercept functions (all panels in the first column of Fig. 5) described the overall trend of the five diffusion properties. Compared with the estimated mean functions using FRATS (Zhu et al., 2010c), they admitted almost identical curves, which indicates the effectiveness of FADTTS. The gender coefficients for MD and all the three eigenvalues (panels (e), (h), (k), and (n) of Fig. 5) are negative at most of the grid points, which may indicate that compared with female infants, male infants have relatively smaller magnitudes of local water diffusivity along the splenium of the corpus callosum. However, the fact that we did observe positive gender effects at some grid point may weaken our findings. We did not observe similar patterns for FA (panel (b) of Fig. 5). The gestational age coefficients for FA (panel (c) of Fig. 5) are positive at most grid points, indicating that FA measures increase with age in both male and female infants, whereas those corresponding to MD and all three eigenvalues (panels (f), (i), (l), and (o) of Fig. 5) are negative at most grid points. This may indicate a negative correlation between the magnitudes of local water diffusivity and gestational age along the splenium of the corpus callosum. It also has been noted that there are negative age effects at some grid points of FA and positive age effects of the other four diffusion properties at some grid points, which again may weaken our findings.

We presented the eigenvalues and eigenfunctions of $\hat{\Sigma}_{\eta,jj}(s, t)$ for all $j = 1, \cdots, J$ in Fig. 6. For all five measures, the relative eigenvalues of $\hat{\Sigma}_{\eta,jj}$ defined as the ratios of the eigenvalues of $\hat{\Sigma}_{\eta,jj}(s, t)$ over their sum have almost identical distributional patterns (panel (a) of Fig. 6). We observed that the first three relative eigenvalues account for 80% of the total and the others quickly vanish to zero. The eigenfunctions of FA corresponding to the largest three eigenvalues (Fig. 6(b)) are different from those of the other four measures (Fig. 6(c)–(f)). For MD, L_1, L_2, and L_3, similar patterns were observed among the eigenfunctions corresponding to the largest three eigenvalues. This is consistent with the fact that FA is a scaled-invariant measure of all the eigenvalues.

We statistically test the effects of gender and gestational age on all five diffusion properties along the splenium tract. To test the gender effect, we calculated the local test statistics $S_n(s_m)$ and their corresponding *p*-values across all grid points on the splenium tract, among which only a few grid points have $-\log_{10}(p)$ values greater than 2 (red line in Fig. 7(a)). Then, we also computed the global test statistic $S_n = 506.69$ and its associated *p*-value ($p = 0.054$), indicating a weakly significant gender effect, which agrees with the findings in panels (e), (h), (k), and (n) of Fig. 5. The $-\log_{10}(p)$ values of $S_n(s_m)$ for testing the age effect at most grid points are greater than 2 (green line in Fig. 7(a)), while a moderately significant age effect was found with $S_n = 971.16$ (*p*-value =.034). This agrees with the findings in panels (c), (f), (i), (l), and (o) of Fig. 5, indicating that some diffusion properties along the splenium tract differ slightly between male and female groups and change moderately with gestational age. Furthermore, for all diffusion properties, we constructed the 95% simultaneous confidence bands of the varying coefficients for G_i and $Gage_i$ (Fig. 5).

For the right internal capsule tract, we have the following findings. Fig. 9 presents the estimated $\hat{B}(s)$ associated with all diffusion properties along the right internal capsule tract (blue solid lines in all panels of Fig. 9). Since the patterns in Fig. 9 were similar to those in Fig. 5, we do not repeat them here. Moreover, for $j = 1, \cdots, 5$, Fig. 10 presents the relative

eigenvalues and eigenvectors of $\hat{\Sigma}_{\eta,jj}(s, t)$ along the right internal capsule tract. As shown in Fig. 10(a), the first three relative eigenvalues account for the 70% of the total, and the rest quickly vanish to zero. For all diffusion properties, the eigenfunctions associated with the largest first eigenvalues for the right capsule tract (panels (b)–(f) of Fig. 10) show patterns similar to those for the splenium tract in Fig. 6. Moreover, we found no significant effect of gender since $S_n = 420.05$ with p-value 0.347, even though the $-\log_{10}(p)$ values of $S_n(s_m)$ for gender are greater than 2 at a few grid points (red line in Fig. 7(b)). However, a highly significant effect of gestational age was found with $S_n = 1549.1$ and its p-value $p < 0.001$, while the $-\log_{10}(p)$ values of $S_n(s_m)$ for the age effect are greater than 2 at all grid points (green line in Fig. 7(b)). This indicates that diffusion properties along the right internal capsule tract do not differ significantly between male and female groups but are significantly associated with gestational age. Finally, we constructed the 95% simultaneous confidence bands of the functional coefficients (Fig. 9).

In our last step, we applied FADTTS to each of the five diffusion properties along both the right internal capsule tract and the splenium tract and then calculated the global test statistic S_n and its associated p-value (Table 2). For the splenium tract, recall the overall p-values $p = 0.054$ and $p = 0.034$ for the gender effect and the age effect, respectively, based on all five diffusion properties. Inspecting individual diffusion properties reveals that gender mainly has a mild effect on MD, L_1 and L_2, while age influences MD and the three eigenvalues. These results agree with the findings in Fig. 9. For the right internal capsule tract, the overall p-values are given by $p = 0.347$ and $p < 0.001$ for the gender effect and the age effect, respectively, based on all the five diffusion properties. We did not observe a gender effect on any of the five individual diffusion properties, but there are significant age effects on all of them.

4. Discussion

The contributions of our work are twofold. From the statistical perspective, we have developed a new functional analysis pipeline for delineating the structure of the variability of multiple diffusion properties along major white matter fiber bundles and their association with a set of covariates of interest. The FADTTS pipeline integrates five advanced statistical tools from the statistical literature. From the application perspective, we have demonstrated FADTTS in a clinical study of neurodevelopment for revealing the complex inhomogeneous spatiotemporal maturation patterns as the apparent changes in fiber bundle diffusion properties. We expect that this novel statistical tool will lead to new findings in our clinical applications.

Several limitations need to be addressed in future research. Even though the three eigenvalues satisfy the constraint $L_1 \geq L_2 \geq L_3$, model (1) and its associated statistical procedure do not impose such a constraint. Moreover, for some strongly nondegenerate tensors ($L_1 \gg L_2 > L_3$) with small L_2 and L_3, there may be difficulty in distinguishing these two smallest eigenvalues. It is also possible that the fitted mean eigenvalues obtained from model (1) may be negative. A possible solution is to require that the fitted eigenvalue in model (1) be non-negative; an alternative solution is to use the logarithm of eigenvalues as responses. Both are topics for future research.

All fiber tract based methods including FADTTS are only applicable to these major white matter tracts in which one can establish the common localization across subjects. Thus, FADTTS is able to investigate a subset of different scenarios in which white matter structure is associated with a covariate, such as age, gender, and diagnostic status. For instance, the centroid of the localization of white matter lesion could vary across time and subjects. In this case, neither ROI based methods nor tract based methods would be appropriate. In some

heterogenous populations, it is possible that tract-specific changes occur in only a subset of subjects.

There are several current topics for our research. We are developing new statistical methods for making statistical inferences about both the eigenvalues and eigenfunctions in FPCA and for establishing the association of eigenvalues and eigenfunctions with a set of covariates of interest. We are exploring other nonparametric methods, such as wavelet and B-spline methods instead of using local polynomial kernel. We are in the process of extending FADTTS to the analysis of high angular resolution diffusion image (HARDI), which is important for resolving the issue of fiber crossing (Lenglet et al., 2009; Tuch et al., 2002). It is also important to extend FADTTS to principal directions and full diffusion tensors on fiber bundles (Schwartzman, 2006; Lepore et al., 2008; Schwartzman et al., 2005; Zhu et al., 2009; Whitcher et al., 2007). The proposed methodology can be readily extended to more complex fiber structures, such as the medial manifolds of fiber tracts (Yushkevich et al., 2008). Furthermore, we will extend FADTTS to longitudinal studies and family studies (Fang and Wang, 2010). Finally, we have treated fiber bundle diffusion properties as functional responses. It will be interesting to consider generalized functional linear models, in which a scalar outcome (e.g., diagnostic group) is used as the response and fiber bundle diffusion properties are used as varying covariate functions (or functional predictor) (Ramsay and Silverman, 2005; Goldsmith et al., 2011).

References

Ashburner J, Friston KJ. Voxel-based morphometry: the methods. Neuroimage. 2000; 11:805–821. [PubMed: 10860804]

Basser PJ, Mattiello J, LeBihan D. Estimation of the effective self-diffusion tensor from the nmr spin echo. Journal of Magnetic Resonance Ser B. 1994a; 103:247–254.

Basser PJ, Mattiello J, LeBihan D. Mr diffusion tensor spectroscopy and imaging. Biophysical Journal. 1994b; 66:259–267. [PubMed: 8130344]

Bonekam D, Nagae LM, Degaonkar M, Matson M, Abdalla WM, Barker PB, Mori S, Horská A. Diffusion tensor imaging in children and adolescents: Reproducibility, hemispheric, and age-related differences. NeuroImage. 2008; 34:733–742.

Camara E, Bodammer N, Rodriguez-Fornells A, Tempelmann C. Age-related water diffusion changes in human brain: A voxel-based approach. NeuroImage. 2007; 34:1588–1599. [PubMed: 17188516]

Cascio CJ, Gerig G, Piven J. Diffusion tensor imaging: Application to the study of the developing brain. J Am Acad Child Adolesc Psychiatry. 2007; 46:213–223. [PubMed: 17242625]

Chen YS, An HY, Zhu HT, Stone T, Smith JK, Hall C, Bullitt E, Shen DG, Lin WL. White matter abnormalities revealed by diffusion tensor imaging in non-demented and demented hiv+ patients. NeuroImage. 2009; 47:1154–1162. [PubMed: 19376246]

Fan, J.; Gijbels, I. Local Polynomial Modelling and Its Applications. Chapman and Hall; London: 1996.

Fan J, Yao Q, Cai Z. Adaptive varying-coefficient linear models. J R Stat Soc Ser B Stat Methodol. 2003; 65(1):57–80.

Fan J, Zhang W. Statistical estimation in varying coefficient models. Ann Statist. 1999; 27(5):1491–1518.

Fan J, Zhang W. Simultaneous confidence bands and hypothesis testing in varying-coefficient models. Scand J Statist. 2000; 27(4):715–731.

Fan J, Zhang W. Statistical methods with varying coefficient models. Stat Interface. 2008; 1(1):179–195. [PubMed: 18978950]

Fang Y, Wang Y. Testing for familial aggregation of functional traits. Statistics in Medicine. 2010

Ferguson CA, Bowman AW, Scott EM, Carvalho L. Multivariate varying-coefficient models for an ecological system. Environmetrics. 2009; 20

Focke NK, Yogarajah M, Bonelli SB, Bartlett PA, Symms MR, Duncan JS. Voxel-based diffusion tensor imaging in patients with mesial temporal lobe epilepsy and hippocampal sclerosis. NeuroImage. 2008; 40:728–737. [PubMed: 18261930]

Ghouch AE, Genton MG. Local polynomial quantile regression with parametric features. Journal of the American Statistical Association. 2009; 104:1416–1429.

Gilmore JH, Smith LC, Wolfe HM, Hertzberg BS, Smith JK, Chescheir NC, Evans DD, Kang C, Hamer RM, Lin W, Gerig G. Prenatal mild ventriculomegaly predicts abnormal development of the neonatal brain. Biol Psychiatry. 2008; 64:1069–1076. [PubMed: 18835482]

Goldsmith A, Feder J, Crainiceanu C, Caffo B, Reich D. Penalized functional regression. Journal of Computational and Graphical Statistics. 2011

Goodlett CB, Fletcher PT, Gilmore JH, Gerig G. Group analysis of dti fiber tract statistics with application to neurodevelopment. NeuroImage. 2009; 45:S133–S142. [PubMed: 19059345]

Gouttard, S.; Prastawa, M.; Bullitt, E.; Lin, W.; Goodlett, C.; Gerig, G. volume 5761 of Lecture Notes in Computer Science. Springer; Berlin/Heidelberg: 2009. Constrained data decomposition and regression for analyzing healthy aging from fiber tract diffusion properties; p. 321-328.

Greven S, Crainiceanu C, Caffo B, Reich D. Longitudinal functional principal component analysis. Electronic Journal of Statistics. 2010; 4:1022–1054.

Hall P, Müller HG, Wang JL. Properties of principal component methods for functional and longitudinal data analysis. Ann Statist. 2006; 34(3):1493–1517.

Hasan KM, Basser PJ, Parker DL, Alexander AL. Analytical computation of the eigenvalues and eigenvectors in dt-mri. J Magn Reson. 2001; 152:41–47. [PubMed: 11531362]

Hasan KM, Narayana PA. Computation of the fractional anisotropy and mean diffusivity maps without tensor decoding and diagonalization: theoretical analysis and validation. Magn Reson Med. 2003; 50:589–598. [PubMed: 12939767]

Hecke WV, Sijbers J, Backer SD, Poot D, Parizel PM, Leemans A. On the construction of a ground truth framework for evaluating voxel-based diffusion tensor mri analysis methods. NeuroImage. 2009; 46:692–707. [PubMed: 19268708]

Jones DK, Symms MR, Cercignani M, Howard RJ. The effect of filter size on vbm analyses of dt-mri data. NeuroImage. 2005; 26:546–554. [PubMed: 15907311]

Kosorok MR. Bootstraps of sums of independent but not identically distributed stochastic processes. J Multivariate Anal. 2003; 84:299–318.

Lenglet C, Campbell JSW, Descoteaux M, Haro G, Savadjiev P, Wassermann D, Anwander A, Deriche R, Pike GB, Sapiro G, Siddiqi K, Thompson PM. Mathematical methods for diffusion mri processing. NeuroImage. 2009; 45:S111–S122. [PubMed: 19063977]

Lepore N, Brun CA, Chou Y, Chiang M, Dutton RA, Hayashi KM, Luders E, Lopez OL, Aizenstein HJ, Toga AW, Becker JT, Thompson PM. Generalized tensor-based morphometry of hiv/aids using multivariate statistics on deformation tensors. IEEE Transactions in Medical Imaging. 2008; 27:129–141.

Li Y, Hsing T. Uniform convergence rates for nonparametric regression and principal component analysis in functional/longitudinal data. The Annals of Statistics. 2010; 38:3321–3351.

Moseley M. Diffusion tensor imaging and aging-a review. NMR Biomed. 2002; 15:553–560. [PubMed: 12489101]

Mukherjee P, McKinstry RC. Diffusion tensor imaging and tractography of human brain development. Neuroimaging Clin N Am. 2006; 16:19–43. [PubMed: 16543084]

O'Donnell L, Westin CF, Golby A. Tract-based morphometry for white matter group analysis. Neuroimage. 2009; 45:832–844. [PubMed: 19154790]

Pierpaoli C, Basser PJ. Toward a quantitative assessment of diffusion anisotropy. Magn Reson Med. 1996; 36:893–906. [PubMed: 8946355]

Ramsay, JO.; Silverman, BW. Springer Series in Statistics. Springer-Verlag; New York: 2002. Applied functional data analysis. Methods and case studies

Ramsay, JO.; Silverman, BW. Functional Data Analysis. Springer-Verlag; New York: 2005.

Rollins NK. Clinical applications of diffusion tensor imaging and tractography in children. Pediatr Radiol. 2007; 37:769–780. [PubMed: 17598098]

Schwartzman, A. PhD thesis. Stanford University; 2006. Random ellipsoids and false discovery rates: Statistics for diffusion tensor imaging data.

Schwartzman A, Dougherty RF, Taylor JE. Cross-subject comparison of principal diffusion direction maps. Magn Reson Med. 2005; 53:1423–1431. [PubMed: 15906307]

Smith SM, Jenkinson M, Johansen-Berg H, Rueckert D, Nichols TE, Mackay CE, Watkins KE, Ciccarelli O, Cader M, Matthews P, Behrens TE. Tractbased spatial statistics: voxelwise analysis of multi-subject diffusion data. NeuroImage. 2006; 31:1487–1505. [PubMed: 16624579]

Snook L, Paulson LA, Roy D, Phillips L, Beaulieu C. Diffusion tensor imaging of neurodevelopment in children and young adults. NeuroImage. 2005; 26:1164–1173. [PubMed: 15961051]

Snook L, Plewes C, Beaulieu C. Voxel based versus region of interest analysis in diffusion tensor imaging of neurodevelopment. NeuroImage. 2007; 34:243–252. [PubMed: 17070704]

Song SK, Sun SW, Ju WK, Lin SJ, Cross AH, Neufeld AH. Diffusion tensor imaging detects and differentiates axon and myelin degeneration in mouse optic nerve after retinal ischemia. Neuroimage. 2003; 20:1714–1722. [PubMed: 14642481]

Tuch DS, Reese TG, Wiegell MR, Makris N, Belliveau JW, Wedeen VJ. High angular resolution diffusion imaging reveals intravoxel white matter fiber heterogeneity. Magnetic Resonance in Medicine. 2002; 48:577–582. [PubMed: 12353272]

Wager TD, Keller M, Lacey SC, Jonides J. Increased sensitivity in neuroimaging analyses using robust regression. Neuroimage. 2005; 26:99–113. [PubMed: 15862210]

Wand, MP.; Jones, MC. Kernel Smoothing. Chapman and Hall; London: 1995.

Wang L, Li H, Huang JZ. Variable selection in nonparametric varying-coefficient models for analysis of repeated measurements. J Amer Statist Assoc. 2008; 103(484):1556–1569.

Welsh AH, Yee TW. Local regression for vector responses. Journal of Statistical Planning and Inference. 2006; 136:3007–3031.

Whitcher B, Wisco JJ, Hadjikhani N, Tuch DS. Statistical group comparison of diffusion tensors via multivariate hypothesis testing. Magnetic Resonance in Medicine. 2007; 57:1065–1074. [PubMed: 17534902]

Worsley KJ, Taylor JE, Tomaiuolo F, Lerch J. Unified univariate and multivariate random field theory. NeuroImage. 2004; 23:189–195.

Wu CO, Chiang CT. Kernel smoothing on varying coefficient models with longitudinal dependent variable. Statist Sinica. 2000; 10(2):433–456.

Wu, HL.; Zhang, JT. Nonparametric Regression Methods for Longitudinal Data Analysis. John Wiley & Sons, Inc; Hoboken, New Jersey: 2006.

Yao F, Lee TCM. Penalized spline models for functional principal component analysis. J R Stat Soc Ser B Stat Methodol. 2006; 68(1):3–25.

Yushkevich PA, Zhang H, Simon T, Gee JC. Structure-specific statistical mapping of white matter tracts. Neuroimage. 2008; 41:448–461. [PubMed: 18407524]

Zellner A. An efficient method of estimating seemingly unrelated regressions and tests for aggregation bias. Journal of the American Statistical Association. 1962; 57:348–368.

Zhang J, Chen J. Statistical inference for functional data. The Annals of Statistics. 2007; 35:1052–1079.

Zhu HT, Cheng YS, Ibrahim JG, Li YM, Hall C, Lin WL. Intrinsic regression models for positive definitive matrices with applications in diffusion tensor images. Journal of the American Statistical Association. 2009; 104:1203–1212. [PubMed: 20174601]

Zhu HT, Ibrahim JG, Tang N, Rowe D, Hao X, Bansal R, Peterson BS. A statistical analysis of brain morphology using wild bootstrapping. IEEE Trans Med Imaging. 2007a; 26:954–966. [PubMed: 17649909]

Zhu, HT.; Li, RZ.; Kong, LL. Technical report. University of North Carolina; Chapel Hill: 2010a. Multivariate varying coefficient models and its applications to neuroimaging data.

Zhu, HT.; Styner, M.; Li, Y.; Kong, L.; Shi, Y.; Lin, W.; Coe, C.; Gilmore, J. volume 6361 of Lecture Notes in Computer Science. Springer: Berlin/Heidelberg; 2010b. Multivariate varying coefficient models for dti tract statistics; p. 690-697.

Zhu HT, Styner M, Tang NS, Liu ZX, Lin WL, Gilmore J. Frats: Functional regression analysis of dti tract statistics. IEEE Transactions on Medical Imaging. 2010c; 29:1039–1049. [PubMed: 20335089]

Zhu HT, Xu D, Amir R, Hao X, Zhang H, Alayar K, Ravi B, Peterson B. A statistical framework for the classification of tensor morphologies in diffusion tensor images. Magnetic Resonance Imaging. 2006; 24:569–582. [PubMed: 16735178]

Zhu HT, Zhang HP, Ibrahim JG, Peterson BG. Statistical analysis of diffusion tensors in diffusion-weighted magnetic resonance image data (with discussion). Journal of the American Statistical Association. 2007b; 102:1085–1102.
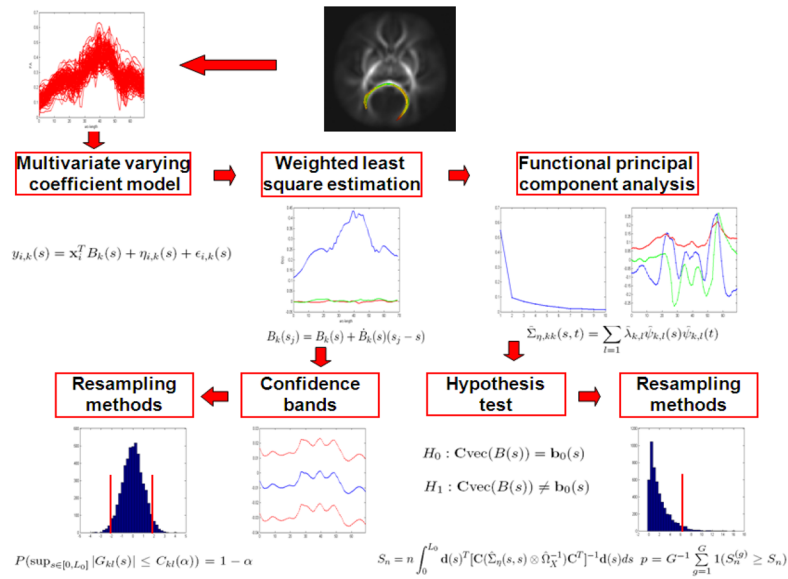
Fig. 1.
A schematic overview of FADTTS: a multivariate varying coefficient model for the diffusion properties of a tract, a weighted least squares method for estimating the coefficient functions, a functional principal component analysis model for analyzing the covariance structure, a hypothesis test for coefficient functions using both local and global test statistics, a resampling method for estimating the p-value of the global test statistics, and a method for constructing the confidence bands of the coefficient functions based on a resampling method.
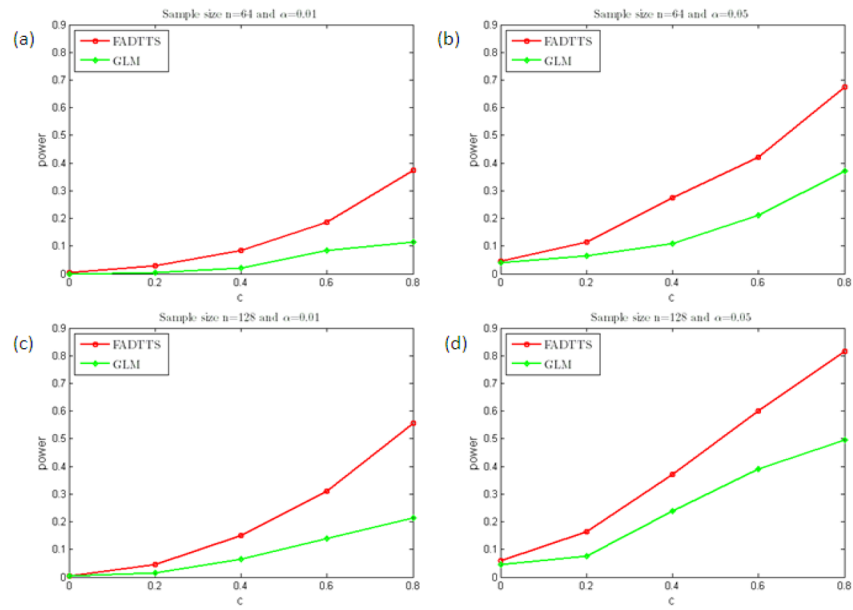
Fig. 2.
Simulation study: Type I and Type II error rates. Rejection rates of S_n based on the resampling method are calculated at five different values of c (representing different effect sizes) for sample sizes $n = 64$ and $n = 128$ at $\alpha = .05$ and $\alpha = .01$ significance levels.
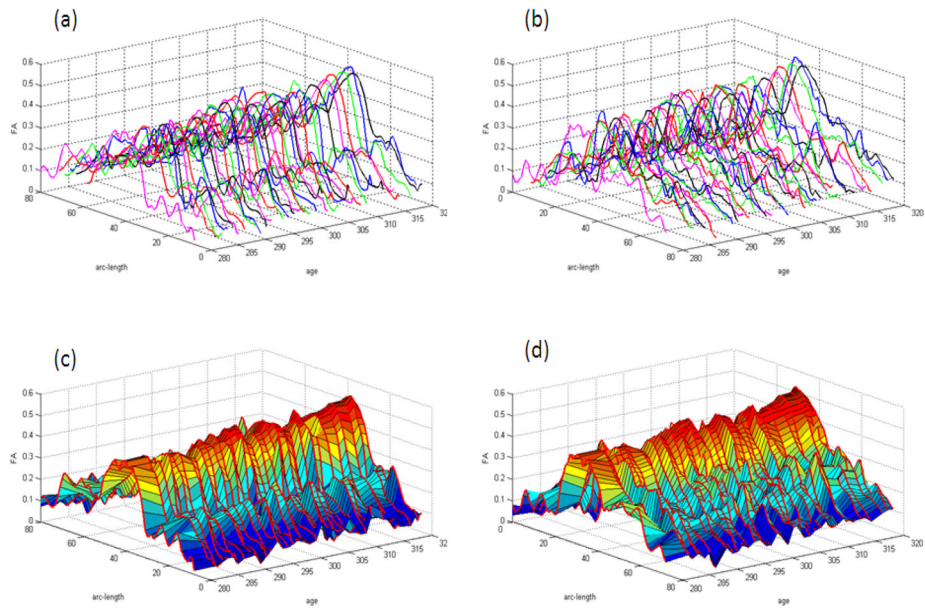
Fig. 3.
3D plots of FA along the right internal capsule tract to illustrate the possible age effect: (a)
and (b) 3D line plot and (c) and (d) 3D surf plot.
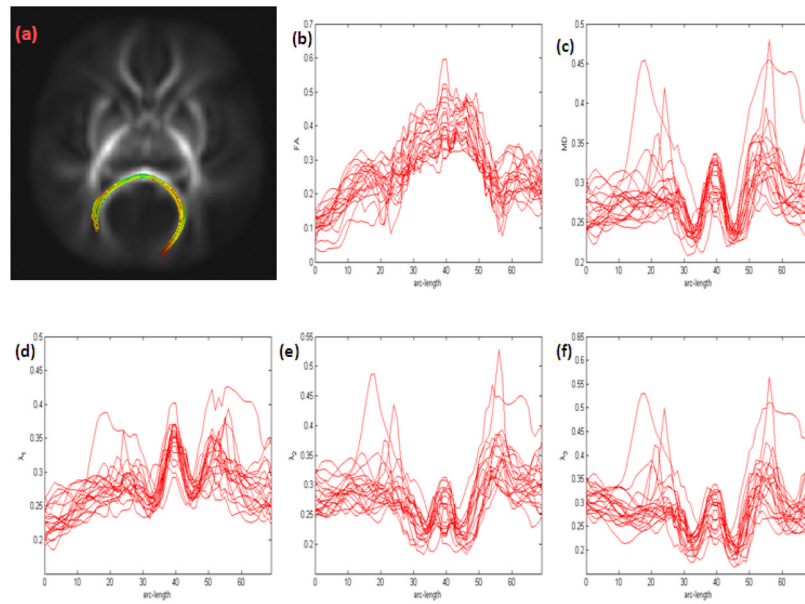
Fig. 4.
Splenium tract and diffusion properties along the splenium tract: (a) The splenium tract
extracted from the tensor atlas with color presenting the mean FA values; (b) FA; (c) MD;
(d) L_1; (e) L_2; and (f) L_3. The diffusion properties in panels (b)–(f) are from 20 randomly
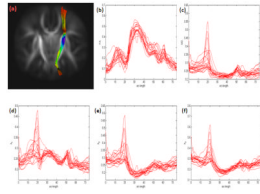selected infants.
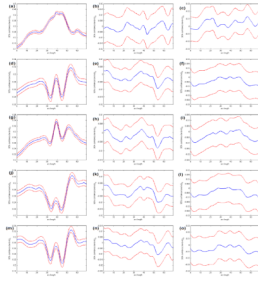
Fig. 5.
The estimated coefficient functions (blue solid lines) and the corresponding 95% confidence bands (red dashed lines) for the five measures along the splenium tract: (a), (d), (g), (j), and (m) the varying intercept functions for FA, MD, L_1, L_2 and L_3, respectively; (b), (e), (h), (k), and (n) the varying coefficient functions of gender for FA, MD, L_1, L_2 and L_3, respectively; (c), (f), (i), (l), and (o) the varying coefficient functions associated with gestational age for FA, MD, L_1, L_2 and L_3, respectively.
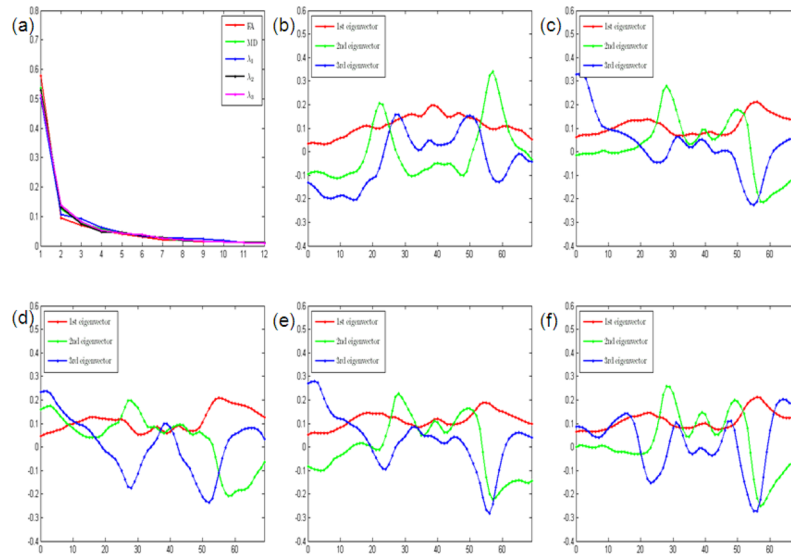
Fig. 6.
Spectral decomposition of $\hat{\Sigma}_{\eta,kk}(s, t)$ for FA, MD, L_1, L_2 and L_3 along the splenium tract: (a) the first 12 relative eigenvalues; (b) the first 3 eigenvectors for FA; (c) the first 3 eigenvectors for MD; (d) the first 3 eigenvectors for L_1; (e) the first 3 eigenvectors for L_2; and (f) the first 3 eigenvectors for L_3.
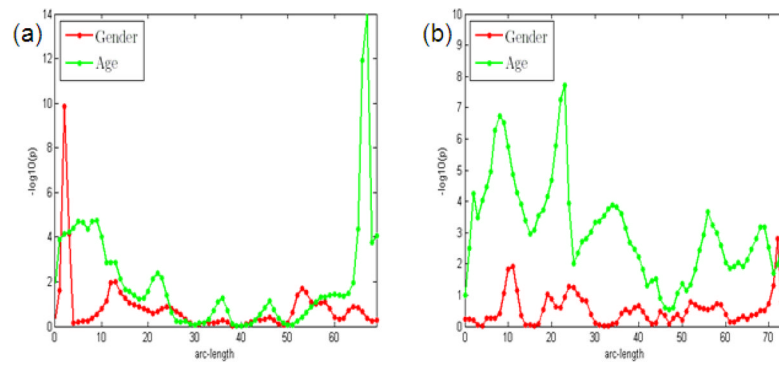
Fig. 7.
$-\log_{10}(p)$ values for testing gender and gestational age effects of test statistics $S_n(s_j)$ for the two selected tracts: (a) $-\log_{10}(p)$ values for testing gender and gestational age effects of the splenium tract; (b) $-\log_{10}(p)$ values for testing gender and gestational age effects of the right internal capsule tract.

Fig. 8.
Right internal capsule and diffusion properties along the right internal capsule tract: (a) the right internal capsule tract extracted from the tensor atlas with color presenting the mean FA values; (b) FA; (c) MD; (d) L_1; (e) L_2; and (f) L_3. The diffusion properties in panels (b)–(f) are from 20 randomly selected infants.
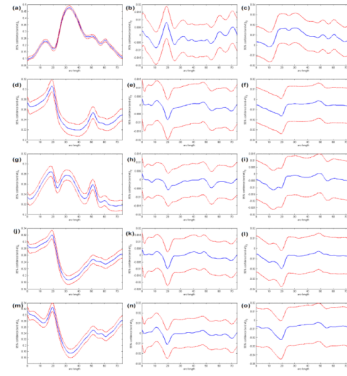
Fig. 9.
The estimated coefficient functions (blue solid lines) and the corresponding 95% confidence bands (red dashed lines) for the five measures along the right internal capsule tract. Panels (a), (d), (g), (j), and (m) are the varying intercept functions for FA, MD, L_1, L_2 and L_3, respectively. Panels (b), (e), (h), (k), and (n) are the varying coefficient functions of gender for FA, MD, L_1, L_2 and L_3, respectively. Panels (c), (f), (i), (l), and (o) are the varying coefficient functions of gestational age for FA, MD, L_1, L_2 and L_3, respectively.
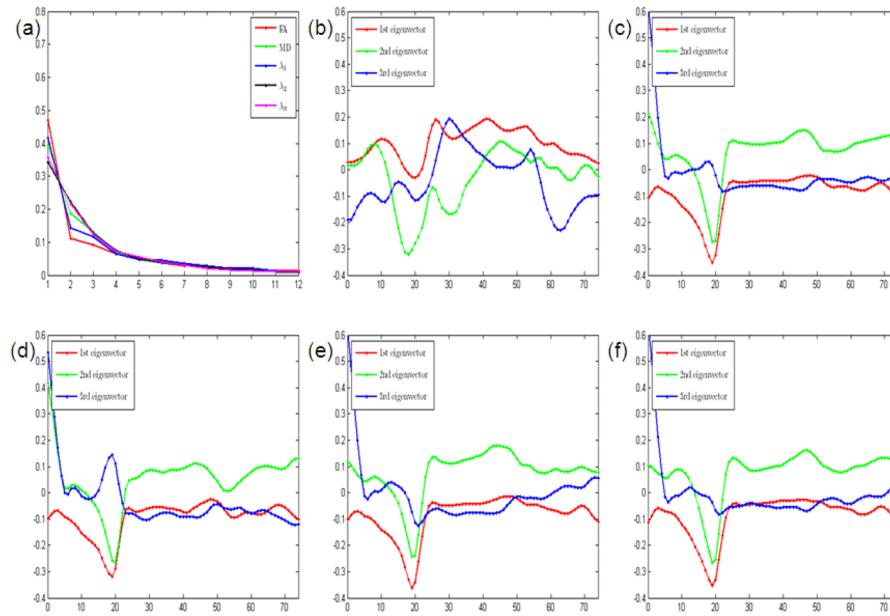
Fig. 10.
Spectral decomposition of $\Sigma_{\eta,kk}(s, t)$ for FA, MD, L_1, L_2 and L_3 along the right internal capsule tract: (a) the first 12 relative eigenvalues for FA, MD, L_1, L_2 and L_3; (b) the first 3 eigenvectors for FA; (c) the first 3 eigenvectors for MD; (d) the first 3 eigenvectors for L_1; (e) the first 3 eigenvectors for L_2; and (f) the first 3 eigenvectors for L_3.

Table 1

Simulation study: the Type I and Type II error rates of S_n under GLM and FADTTS.

	Sample size n=64				Sample size n=128			
	$\alpha = 0.01$		$\alpha = 0.05$		$\alpha = 0.01$		$\alpha = 0.05$	
	GLM	FADTTS	GLM	FADTTS	GLM	FADTTS	GLM	FADTTS
c=0.000	0.000	0.005	0.040	0.045	0.005	0.005	0.045	0.060
c=0.200	0.005	0.030	0.065	0.115	0.015	0.045	0.075	0.165
c=0.400	0.020	0.085	0.110	0.275	0.065	0.150	0.240	0.370
c=0.600	0.085	0.185	0.210	0.420	0.140	0.310	0.390	0.600
c=0.800	0.115	0.375	0.370	0.675	0.215	0.555	0.495	0.815

The *p*-values of S_n for testing the effects of gender and gestational age on the splenium and right internal capsule tracts.

	Splenium		Right internal capsule	
	gender	gestational age	gender	gestational age
FA	0.683	0.103	0.169	<0.001
MD	0.063	0.008	0.354	<0.001
L_1	0.048	0.003	0.241	<0.001
L_2	0.057	0.007	0.314	<0.001
L_3	0.302	0.010	0.376	<0.001
(FA, MD, L_1, L_2, L_3)	0.054	0.034	0.347	<0.001